Archives of Hydro-Engineering and Environmental Mechanics
Vol. 51 (2004), No. 1, pp. 3–24

Two-Dimensional Modelling of Wave Motion in Shallow-Water Areas

Jarosław Kapiński

Institute of Hydro-Engineering of the Polish Academy of Sciences
ul. Kościerska 7, 80-953 Gdańsk, Poland, e-mail: Kapinski@ibwpan.gda.pl

(Received April 04, 2002; revised October 02, 2003)

Abstract

A new mathematical model for prediction of a two-dimensional wave motion in shallow water is presented herein. It can be applied to investigate shoaling, diffraction, refraction, breaking, bottom friction and wave run-up on a beach, as well as mass transport and orbital motion. The model also includes an oblique wave approach to the shore and irregular bottom topography. Such engineering constructions as seawalls, breakwaters and groins are simulated numerically. Simple results of computations, shown in graphic form, indicate possible practical applications of the model.

Key words: swash zone, shallow water, wave transformation, Lagrangian approach, two-dimensional model

Notation

c	–	shallow-water wave celerity,
f	–	bottom friction coefficient used in a quadratic formula,
f_V	–	bottom friction coefficient used in a linear formula,
$\overline{F^L}$	–	sum of all forces acting on a water parcel,
g	–	gravitational acceleration,
h	–	water depth at point $P(x, y)$,
$h_{\max}$	–	maximum water depth,
h_{x0}	–	water depth along the onshore boundary,
h_{xB}	–	water depth along the offshore boundary,
h_{y0}	–	water depth along the left-side boundary,
h_{yB}	–	water depth along the right-side boundary,
h^L	–	water depth at point $P(x^L, y^L)$,
H	–	incident wave height,

i – indication of a node at numerical grid in X direction,
$\overline{i}$ – unit vector parallel to X direction,
j – indication of a node at numerical grid in Y direction,
$\overline{j}$ – unit vector parallel to Y direction,
k – wave number,
l_x – length of the left- and right-side boundary,
l_y – length of the onshore and offshore boundary,
L – incident wavelength,
m^L – mass of a water parcel,
p – water pressure at point $P(x, y)$,
p_0 – air pressure,
p^L – water pressure at point $P(x^L, y^L)$,
$\overline{p^L}$ – momentum of a water parcel,
$P(x, y)$ – position of a parcel till initial instant $t = 0$,
$P(x^L, y^L)$ – position of a parcel at time t,
$\overline{R}$ – wave radius,
R_{down} – maximum wave run-down height,
R_{up} – maximum wave run-up height,
S_{br} – critical surface steepness of a wave front,
S^L – surface projection of a water parcel on XY plane,
SWL – still water level,
t – time,
T – wave period,
$\overline{v}$ – flow velocity at point $P(x, y)$,
$\overline{v^L}$ – flow velocity at point $P(x^L, y^L)$ i.e. water parcel velocity,
$\overline{v^L_{x0}}$ – horizontal component of velocity of a water tongue tip,
V^L – volume of a water parcel,
x – cross-shore co-ordinate, component of a parcel position to $t = 0$ as well,
x^L – cross-shore component of a parcel position,
y – longshore co-ordinate, component of a parcel position till $t = 0$ as well,
y^L – longshore component of a parcel position,
z – vertical co-ordinate,
α – angle of a uniformly sloped bottom,
β – angle of wave incidence at the offshore boundary,

Δt – time step,
Δx – mesh spacing in X direction,
Δy – mesh spacing in Y direction,
ζ – water surface elevation at point $P(x, y)$,
ζ_{x0} – water surface elevation at junction of SWL with a bottom slope, i.e. at $P(x = 0, y)$,
ζ_{x0}^{L} – vertical displacement of a water tongue tip,
ζ^{L} – water surface elevation at point $P(x^L, y^L)$,
ξ – cross-shore component of displacement of a parcel,
ξ_{x0} – cross-shore component of displacement of a water tongue tip,
ρ – water density,
$\overline{\rho}$ – displacement of a parcel,
$\overline{\tau}$ – bottom shear stress at point $P(x, y)$,
$\overline{\tau^{L}}$ – bottom shear stress at point $P(x^L, y^L$,
ψ – longshore component of displacement of a parcel,
ψ_{x0} – longshore component of displacement of a water tongue tip,
ω – angular frequency.

1. Introduction

Previous works (Kapiński and Kołodko 1996, Kapiński 2003) have presented a mathematical model for prediction of a surface wave motion in shallow water. The subject of the analysis were one-dimensional waves approaching the shore over a varying bottom depth. Dissipation of wave energy was modelled in the form of bottom friction and bore-like breaking. For the simulation of shear stress at the bottom, two formulas were tested. In the first case, the shear stress depended linearly on depth-averaged parcel velocity and in the second one quadratic dependence was employed. The wave breaking phenomenon was predicted as a moving hydraulic jump (bore). It was realized by reducing a local surface gradient at the wave front. In consequence, the maximum inclination of the wave front did not excess a given value and a breaking wave height diminished towards the shoreline.

The main property of the model, however, distinguishing it from other models, is a hybrid Lagrangian-Eulerian approach to the description of a wave and wave-induced water motion. Governing equations are derived on the basis of momentum and mass conservation laws expressed in the Lagrangian sense, but some further analysis is carried out in the Eulerian meaning. One of the advantages of the model, resulting from the adopted approach, is a direct description of water particle displacements (trajectories) and, in consequence, of their velocities and

accelerations. Another property is the accuracy of modelling of moving boundaries. It is especially interesting in the case of precise prediction of hydrodynamic phenomena that occur at the shoreline, e.g. wave uprush-backwash, wave reflection and interference with oncoming waves. Moreover, the hybrid treatment of the governing equations enables us to identify mass transport as a down-wave mean flow velocity. All these phenomena, although modelled simultaneously, can be analysed separately or jointly depending on a formulated problem.

This paper takes into account a two-dimensional mathematical model for prediction of a wave motion in the shallow-water area. The newly elaborated model is a development of the aforementioned description into the longshore direction. It enables analysis of different phenomena related to an oblique wave propagation and run-up on a beach slope, as well as resulting water and orbital motion over a two-dimensional bottom. Obviously, all properties of the one-dimensional model are retained. For the simplest hydrodynamic and bathymetrical condition classical wave equations are derived, whereas for a more general case a numerical model has been elaborated. Selected results of simple numerical computations are also given.

2. Theoretical Background

2.1. Fundamental Equations

A detailed description of the preceding model, on which the current description is based, can be found in Kapiński (2003). Herein, only the main principles are repeated and next an introduction to a two-dimensional Lagrangian-Eulerian approach is given.

Water flow, for which physical continuity is assumed, is observed in relation to the Cartesian orthogonal co-ordinate system. The system is expressed in a Eulerian sense i.e. its co-ordinates are fixed in space. In general, the description presented in this paper remains in compliance with the so-called de Saint Venant model for which inviscid water and vertically linear distribution of pressure are taken. In addition, propagating waves have to satisfy the condition of small vertical parcel accelerations.

A sketch of the model is shown in Fig. 1. Vertical Z-axis intersects the offshore-directed X-axis at the junction of SWL (still water level) with the beach, and the Y-axis is laid at the straight shoreline. The initial and current position of a selected water parcel is painted in grey. Depth, water surface elevation and bottom shear stress at the motionless position $P(x, y)$, occupied by the selected parcel until initial instant, are denoted as h, ζ and τ_{fr}, respectively, whereas the parameters corresponding to a moving parcel position $P(x^L, y^L)$ are signed by the superscript L i.e.: h^L, ζ^L and τ_{fr}^L. A displacement of a parcel is given as $\overline{\rho} = \overline{\rho}\{\xi, \psi\}$, where ξ and ψ are the perpendicular and parallel to the shore horizontal components. In a similar way, water elevation at $P(x = 0, y)$ is denoted as $\zeta_{x0} = \zeta(t, x = 0, y)$.

Parcels occupying this position till initial instant, $t \leq 0$, describe excursion of a water tongue tip on a beach. Their displacements are denoted as $\overline{\rho_{x0}} = \overline{\rho}\{\xi_{x0}, \psi_{x0}\}$, showing also instantaneous tongue tip elevation ζ_{x0}^L as well as maximum run-up and run-down heights in the extreme positions: $R_{up} = \max \zeta_{x0}^L$, $R_{down} = \min \zeta_{x0}^L$. Additionally, water depths below *SWL* (i.e. for $z < 0$) are taken as positive. Figure 2 may also be useful in visualisation of some parameters related to a parcel, treated here as an elementary particle in a kinematic environment.

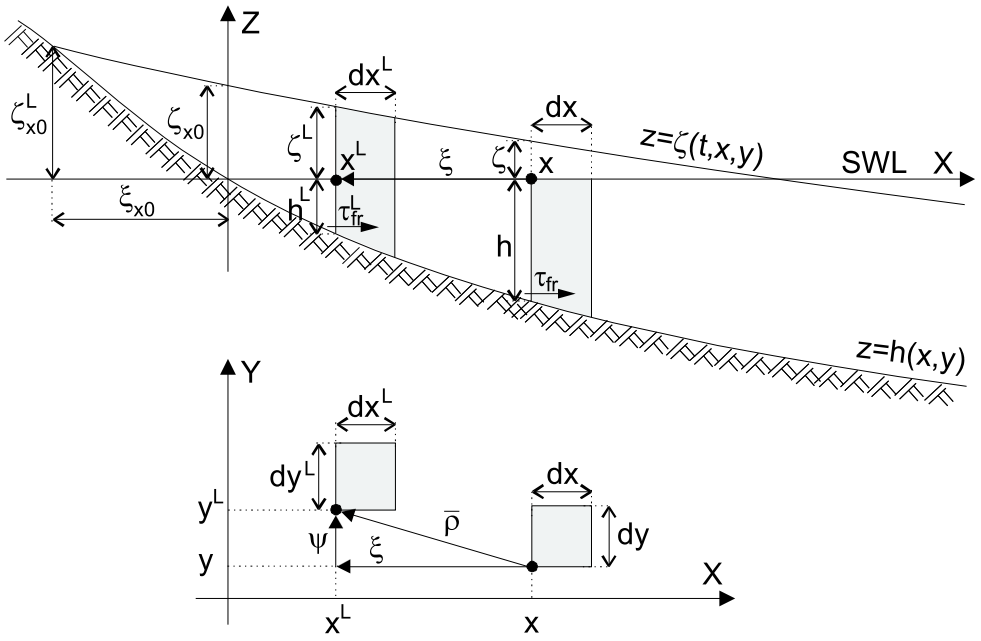

Fig. 1. Sketch of the model

The equations complying with the momentum and mass conservation laws, expressed in the Lagrangian meaning, are as follows:

$$\frac{D}{Dt}\overline{p^L} = \overline{F^L}, \tag{1}$$

$$\frac{D}{Dt}m^L = 0, \tag{2}$$

where:

$$\overline{p^L} = \int\limits_{m^L} \overline{v^L} dm^L = \int\limits_{V^L} \rho^L \overline{v^L} dV^L, \tag{3}$$

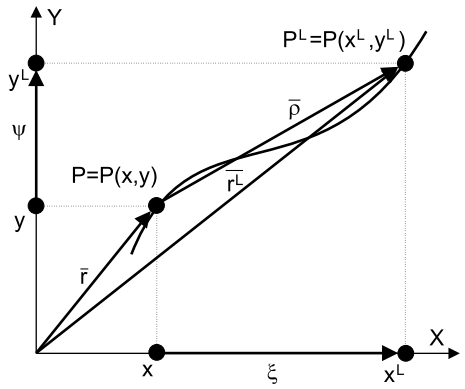

Fig. 2. Sketch of particle displacement

$$m^L = \int_{V^L} \rho^L dV^L, \tag{4}$$

$\frac{D}{Dt}$ – Stokes operator,

$\overline{p^L}, \overline{v^L}, m^L, \rho^L$ – momentum, velocity, mass and mass density of a travelling parcel,

$\overline{F^L}$ – sum of all forces acting on a parcel.

Because of the assumption of incompressibility, ρ^L is taken to be constant for all parcels and in the forthcoming analysis, for shortening of notation, it will be denoted as ρ.

The model presented assumes two-dimensional, depth-averaged water flow. Thus, water and orbital velocities are described as follows:

$$\overline{v} = \frac{1}{h+\zeta} \int_h^\zeta \overline{v}\,(t, x, y, z)\, dz, \tag{5}$$

$$\overline{v^L} = \frac{\partial \overline{\rho}}{\partial t} = \frac{1}{h^L + \zeta^L} \int_{h^L}^{\zeta^L} \overline{v^L}\left(t, x^L, y^L, z^L\right) dz. \tag{6}$$

Assumptions of non-viscidity and small vertical accelerations give:

$$p^L = p_0 + \rho g\left(\zeta^L - z^L\right). \tag{7}$$

Moreover, external surface forces in the model have been limited to the action of friction at the bottom and bore-like breaking at the free water surface. Thus, we have:

$$\overline{F_V^L} = \overline{\tau_{fr}^L} S^L + \overline{\tau_{br}^L} S^L, \tag{8}$$

where the bottom surface S^L can be described by the following equation with sufficient accuracy (cf. Fig. 4):

$$S^L = d_x x^L d_y y^L. \tag{9}$$

Now, the conservation equations (1) and (2), adjusted to the model conditions, assume the following form:

$$\begin{aligned} &\rho \left(h^L + \zeta^L\right) d_x x^L d_y y^L \frac{\partial^2 \overline{\rho}}{\partial t^2} = \\ &= -\left(h^L + \zeta^L\right) d_x x^L d_y y^L \mathrm{grad} p^L + \overline{\tau_{fr}^L} d_x x^L d_y y^L + \overline{\tau_{br}^L} d_x x^L d_y y^L, \end{aligned} \tag{10}$$

$$\rho h dx dy = \rho \left(h^L + \zeta^L\right) d_x x^L d_y y^L, \tag{11}$$

where:

$$d_x x^L = \frac{\partial x^L}{\partial x} dx = \frac{\partial \left(x + \xi\right)}{\partial x} dx = \left(1 + \frac{\partial \xi}{\partial x}\right) dx, \tag{12}$$

$$d_y y^L = \frac{\partial y^L}{\partial y} dy = \frac{\partial \left(y + \psi\right)}{\partial y} dy = \left(1 + \frac{\partial \psi}{\partial y}\right) dy. \tag{13}$$

The formulas for bottom shear stress and wave breaking employed here have been rewritten from the one-dimensional model (Kapiński, 2003) and adapted to the two-dimensional conditions:

– linear bottom friction $\left(\overline{\tau_{fr}^L} \sim \overline{v^L}\right)$:

$$\overline{\tau_{fr}^L} = -f_V \rho h \frac{\partial \overline{\rho}}{\partial t}, \tag{14}$$

where: $[f_V]$=1/s and $f_V \ll \omega$ (after Voltzinger et al 1989),

– quadratic bottom friction $\left(\overline{\tau_{fr}^L} \sim \left(\overline{v^L}\right)^2\right)$:

$$\overline{\tau_{fr}^L} = -\frac{1}{2} f \rho \left|\frac{\partial \overline{\rho}}{\partial t}\right| \frac{\partial \overline{\rho}}{\partial t}, \tag{15}$$

– bore-like breaking:

$$\overline{\tau_{br}^L} = \begin{cases} 0, & \mathrm{grad}\zeta^L \le S_{br} \\ \rho g h \left(\mathrm{grad}\zeta^L - S_{br}\right), & \mathrm{grad}\zeta^L > S_{br} \end{cases}, \tag{16}$$

where:

$$\text{grad}\ \zeta^L = \frac{\partial \zeta^L}{\partial x^L}\overline{i} + \frac{\partial \zeta^L}{\partial y^L}\overline{j} = \frac{\dfrac{\partial \zeta^L}{\partial x}}{1+\dfrac{\partial \xi}{\partial x}}\overline{i} + \frac{\dfrac{\partial \zeta^L}{\partial y}}{1+\dfrac{\partial \psi}{\partial y}}\overline{j}, \tag{17}$$

S_{br} – critical surface steepness of a wave front responsible for dissipation intensity,

$\overline{i}, \overline{j}$ – unit vectors in X and Y direction, respectively.

The term (16), included to the governing equations, does not permit steepening of the wave front over a chosen value S_{br}.

After simple rearrangement of (10) and (11) we have a set of three scalar equations:

$$\frac{\partial^2 \xi}{\partial t^2} = -g\frac{\dfrac{\partial \zeta^L}{\partial x}}{1+\dfrac{\partial \xi}{\partial x}} + \frac{\tau^L_{frx} + \tau^L_{brx}}{\rho\left(h^L + \zeta^L\right)}, \tag{18}$$

$$\frac{\partial^2 \psi}{\partial t^2} = -g\frac{\dfrac{\partial \zeta^L}{\partial y}}{1+\dfrac{\partial \psi}{\partial y}} + \frac{\tau^L_{fry} + \tau^L_{bry}}{\rho\left(h^L + \zeta^L\right)}, \tag{19}$$

$$\zeta^L = \frac{h}{\left(1+\dfrac{\partial \xi}{\partial x}\right)\left(1+\dfrac{\partial \psi}{\partial y}\right)} - h^L, \tag{20}$$

with three unknown quantities: ξ and ψ which denote components of a parcel displacement since the initial position $P(x, y)$ and ζ^L as a water surface elevation corresponding to the current position of the parcel $P(x^L, y^L)$.

2.2. Simplifying Assumptions

To obtain the solution of the set of Eqs. (18), (19) and (20), two simplifying assumptions are adapted to the model. The first assumption imposes small differences in displacements of neighbouring parcels, however, magnitudes of the displacements of the parcels are not limited. It can be written as follows:

$$\left(\frac{\partial \overline{\rho}}{\partial \overline{r}}\right)^2 \ll 1, \tag{21}$$

where: $\overline{\rho} = \overline{\rho}\{\xi, \psi\}$, $\overline{r} = \overline{r}\{x, y\}$,

or in scalar notation:

$$\left(\frac{\partial \xi}{\partial x}\right)^2 \ll 1, \left(\frac{\partial \psi}{\partial y}\right)^2 \ll 1. \tag{22}$$

Now, the following condition can be adopted to the model as valid:

$$\frac{1}{1+\dfrac{\partial \overline{\rho}}{\partial \overline{r}}} = 1 - \frac{\partial \overline{\rho}}{\partial \overline{r}}. \tag{23}$$

The scalar equivalent to (23) is:

$$\frac{1}{1+\dfrac{\partial \xi}{\partial x}} = 1 - \frac{\partial \xi}{\partial x}, \quad \frac{1}{1+\dfrac{\partial \psi}{\partial y}} = 1 - \frac{\partial \psi}{\partial y}. \tag{24}$$

The second simplification is connected with a bottom surface for which the following condition is imposed:

$$\left|\frac{\partial^2 h}{\partial \overline{r}^2}\right| \ll \frac{h^L}{\overline{\rho}^2}, \tag{25}$$

where: $h = h\,(x, y)$.

The scalar form of (25) is:

$$\left|\frac{\partial^2 h}{\partial x^2} + 2\frac{\partial^2 h}{\partial x\,\partial y} + \frac{\partial^2 h}{\partial y^2}\right| \ll \frac{h^L}{\xi^2 + \psi^2}. \tag{26}$$

As a consequence of (26), an expansion of a water depth $h^L = h^L\,(x + \xi, y + \psi)$ in the Taylor series can be shortened to the form:

$$h^L = h + \xi\frac{\partial h}{\partial x} + \psi\frac{\partial h}{\partial y}. \tag{27}$$

Taking the condition (26) into account, two kinds of bathymetry are acceptable in the model:

- plane bottoms including horizontal, gently inclined or steep slopes,
- non-planar, gently bending bottoms also with inflexion points included.

This means that barred bottoms as well as submarine ridges and canyons can be modelled, however, both aforementioned limitations have to be satisfied then. In addition, a boundary condition at the shoreline, describing a vertical wall, has been derived numerically. This enables prediction of a wave motion in the case of a vertical cliff or a seawall founded on the sea bed. Selected examples of acceptable bathymetry are sketched in Fig. 3.

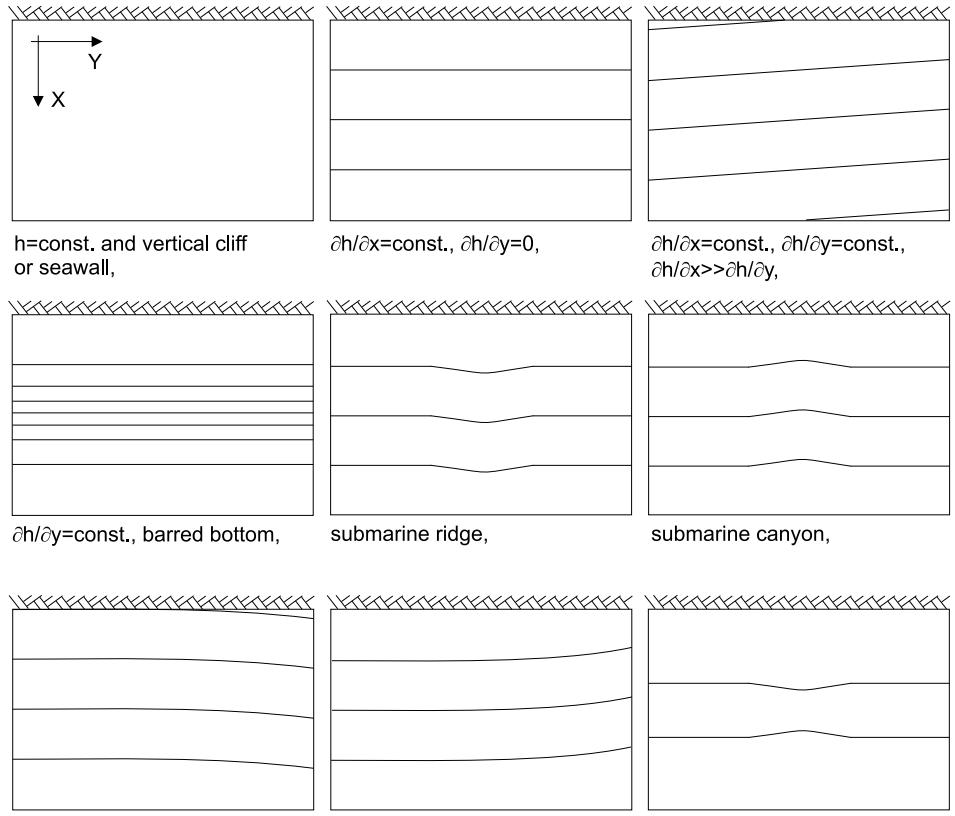

Fig. 3. Examples of simple bathymetry

2.3. Governing Equations

The substitution of (24) and (20) into (18) and (19) and subsequently dropping negligible terms down yields:

$$\frac{\partial^2 (h\xi)}{\partial t^2} = -gh\frac{\partial \zeta^L}{\partial x} + \frac{\tau^L_{frx} + \tau^L_{brx}}{\rho}, \tag{28}$$

$$\frac{\partial^2 (h\psi)}{\partial t^2} = -gh\frac{\partial \zeta^L}{\partial y} + \frac{\tau^L_{fry} + \tau^L_{bry}}{\rho}. \tag{29}$$

Whereas the substitution of (24) and (27) into (20) gives:

$$-\zeta^L = \frac{\partial (h\xi)}{\partial x} + \frac{\partial (h\psi)}{\partial y}. \tag{30}$$

The combination of differentiated (28) after x, (29) after y and double differentiated (30) after t yields:

$$\frac{\partial^2 \zeta^L}{\partial t^2} = g\frac{\partial\left(h\dfrac{\partial \zeta^L}{\partial x}\right)}{\partial x} + g\frac{\partial\left(h\dfrac{\partial \zeta^L}{\partial y}\right)}{\partial y} - \frac{\dfrac{\partial\left(\tau^L_{frx} + \tau^L_{brx}\right)}{\partial x} + \dfrac{\partial\left(\tau^L_{fry} + \tau^L_{bry}\right)}{\partial y}}{\rho}. \quad (31)$$

A set of Eqs. (28), (29) and (31) constitutes a complete description of a wave and water parcel motion. Moreover, on the basis of displacements of parcels $\overline{\rho} = \overline{\rho}\,(t, x, y)$, flow velocity $\overline{v} = \overline{v}\,(t, x, y)$ in the whole computational domain is calculated. The motion of both plane and circular waves can be simulated here, however, in this paper, analysis has been restricted to the first type only.

To confirm correctness of the governing equations a simple derivation is given below. Taking a constant water depth into account, $h = \text{const.}$, and neglecting the loss of wave energy $\overline{\tau_{fr}} = \overline{\tau_{br}} = 0$, Eq. (31) may be simplified to the form:

$$\frac{\partial^2\left(h\zeta^L\right)}{\partial t^2} = gh\frac{\partial^2\left(h\zeta^L\right)}{\partial x^2} + gh\frac{\partial^2\left(h\zeta^L\right)}{\partial y^2}, \quad (32)$$

where the term gh is shallow-water wave celerity c.

For the same assumptions, the substitution of (30) into (28) and (29) yields:

$$\frac{\partial^2 \xi}{\partial t^2} = -gh\frac{\partial^2 \xi}{\partial x^2}, \quad (33)$$

$$\frac{\partial^2 \psi}{\partial t^2} = -gh\frac{\partial^2 \psi}{\partial y^2}. \quad (34)$$

Equations (32), (33) and (34) are one- and two-dimensional forms of the classic wave equation, respectively. They are the simplest description of mechanical disturbances spreading in a uniform medium.

3. Numerical Model

3.1. Grid Formulation

As mentioned, an Eulerian co-ordinate system has been adopted in the model. The computational area, taken until initial instant as a rectangle, is covered by a "stretching" grid system in which nodes travel with corresponding to them local flow velocities. This means that initially rectangular meshes are experienced in displacement and deformation i.e. they are expressed in the Lagrangian sense. A sketch of the mesh used in the model is shown in Fig. 4. Governing equations (28), (29) and (31) have been solved numerically by means of the finite difference method in which an explicit scheme is used.

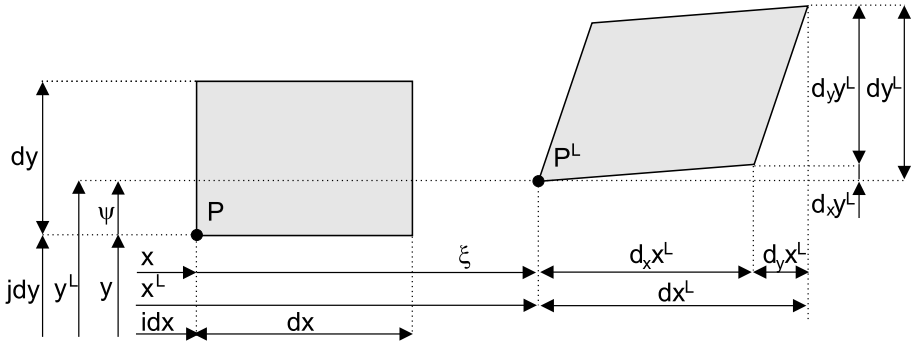

Fig. 4. Transformation of an initially rectangular mesh

3.2. Stability Criterion

Numerical stability requirement for the difference approximation of Eq. (31) is taken after Potter (1973) and adjusted to the model conditions:

$$\Delta t < 0.9\sqrt{\frac{\Delta x^2 + \Delta y^2}{2gh_{\max}}} \approx 0.2\sqrt{\frac{\Delta x^2 + \Delta y^2}{h_{\max}}}, \tag{35}$$

where:

Δt – time step,
$\Delta x, \Delta y$ – mesh spacing to initial instant, $t = 0$, in X and Y direction, respectively,
$h_{\max}$ – maximum water depth.

For simplicity, only the value of a wave celerity $c_{\max} = \sqrt{gh_{\max}}$ has been taken here. It enables to assume a constant time step of computations Δt in the whole numerical grid. The coefficient equal to 0.9 in Eq. (35) is based on numerical experiments and takes into account the maximum contraction of meshes during computations in relation to their initial size.

3.3. Boundary Conditions

Quite different conditions exist at boundaries surrounding the computational domain. The bottom surface is assumed to be rigid (i.e. motionless) $h = h(x, y)$ and impermeable. Whereas at the free water surface a constant air pressure, $p_0 =$ const., is taken. An initial landward boundary agrees with the straight shoreline (cf. Fig. 5). For the condition $h(x = 0, y) = 0$, Eq. (31) simplifies to the form:

$$\frac{\partial^2 \zeta_{x0}^L}{\partial t^2} = g\frac{\partial h_{x0}}{\partial x}\frac{\partial \zeta_{x0}^L}{\partial x} - \frac{1}{\rho}\left(\frac{\partial\left(\tau_{frx}^L + \tau_{brx}^L\right)}{\partial x} + \frac{\partial\left(\tau_{fry}^L + \tau_{bry}^L\right)}{\partial y}\right). \tag{36}$$

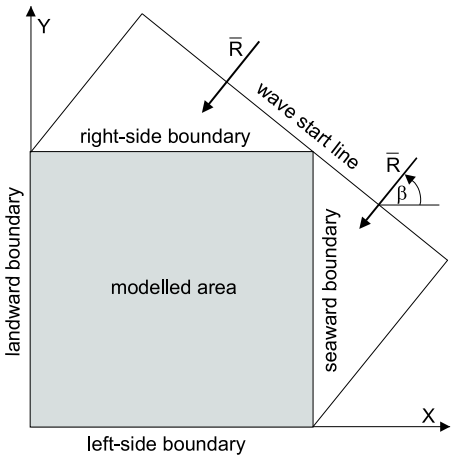

Fig. 5. Side boundaries in a numerical model

It is worth emphasising here, that Eq. (36) is derived from a general equation governing wave motion and no additional assumptions or numerical tricks are used at the landward moving boundary. Equation (36) is expanded with a forward difference approximation, contrary to the interior of the computational area, where a centred difference analogue is used.

The left-side boundary is assumed as a permeable due to wave and water motion and the following condition is adopted:

$$\frac{\partial \zeta_{y0}^{L}}{\partial y} = \text{const.} \tag{37}$$

Thus neighbouring nodes outside the computational area at each time step of computations are described as follows:

$$\zeta_{i,j=-1}^{L} = 2\zeta_{i,j=0}^{L} - \zeta_{i,j=1}^{L}, \tag{38}$$

where:

i – node number in X direction, $i = 0, 1, 2,...,I-1, I$,

j – node number in Y direction, $j = 0$ corresponds to all nodes on the left-hand boundary.

At the seaward boundary a small-amplitude wave motion is generated. Waves appear and start their motion at the line indicated in Fig. 5 as the *wave start line*, therefore they arrive to the boundary with both a delay and partially developed water elevation. The boundary condition is as follows:

$$\zeta_{xB}^{L} = \zeta^{L}(t, x = l_x, y) =$$

$$= \begin{cases} \dfrac{H}{2} \sin\left[\omega\left(t - \dfrac{(l_y - y)}{\sqrt{g h_{xB}}} \sin\beta\right)\right], & t \geq \dfrac{(l_y - y)}{\sqrt{g h_{xB}}} \sin\beta \\ 0, & t < \dfrac{(l_y - y)}{\sqrt{g h_{xB}}} \sin\beta \end{cases}, \tag{39}$$

where:

β – angle of wave incidence,
h_{xB} – depth at the offshore boundary,
l_x – length of the left- and right-hand boundary,
l_y – length of the landward and seaward boundary.

By analogy, the condition at the right-hand boundary is derived as follows:

$$\zeta_{yB}^{L} = \zeta^{L}(t, x, y = l_y) =$$

$$= \begin{cases} \dfrac{H}{2} \sin\left[\omega\left(t - \dfrac{(l_x - x)}{\sqrt{g h_{yB}}} \cos\beta\right)\right], & t \geq \dfrac{(l_x - x)}{\sqrt{g h_{yB}}} \cos\beta \\ 0, & t < \dfrac{(l_x - x)}{\sqrt{g h_{yB}}} \cos\beta \end{cases}, \tag{40}$$

where:

h_{yB} – water depth on the right-hand boundary.

Conditions (39) and (40) have been written for the simplest case, i.e. constant depth along the boundaries. For an arbitrary depth the equations are much more complex and will thus be dropped here.

The initial condition assumes no motion and still water level (SWL) by time $t = 0$:

$$\xi(t \leq 0, x, y) = \psi(t \leq 0, x, y) = \zeta^{L}(t \leq 0, x, y) = 0, \tag{41}$$

where: $x \in < 0, l_x >$, $y \in < 0, l_y >$.

4. Examples of Numerical Solutions

Several results of numerical computations are presented herein. They are purposely given for simplified wave and bathymetric conditions, to show simulated phenomena pellucidly. In all examples sinusoidal wave trains are generated at the seaward boundary with height $H = 1.0$ m and period $T = 10$ s. They are spreading in a numerical tank filled with water at rest by the initial time $t = 0$. Moreover, space and time steps of numerical computations amount to $\Delta x = \Delta y = 1.0$ m, $\Delta t = 0.1$ s, respectively.

The simplest example is shown in Fig. 6. where waves approach the shore perpendicularly over a uniformly sloping bottom. The bathymetry is sketched in Fig. 6A, whereas Figs. 6B and 6C show the wave train at time $t=15$ s of its propagation. The succeeding pictures (Figs. 6D and 6E) give different stages of wave run-up and run-down. The modelled area is a 150 metres square. As the propagation can be simulated with a 1D model, the wave profiles are identical for any cross-section. It is worth emphasising that no numerical disturbances appear at the boundaries.

The aim of the next example is to show the refraction of a wave train in the case of a non-uniform bottom depth. The bathymetry is shown in Figs. 7A, 7B and 7C, whereas the transformation of a wave profile is given in Figs. 7D and 7E. Bottom surface is described with the function:

$$h = -4 + \sin\left(\pi \frac{x}{150}\right) \times \sin\left(\pi \frac{y}{150}\right), \tag{42}$$

giving the maximum elevation in the middle point of the square. Noticeable bends of lines of constant water elevation are observed here. They indicate a slower wave celerity at smaller water depths.

The succeeding example shows an oblique wave motion in a basin with a constant water depth ($h = 4.0$ m) ending in a vertical wall (cf. Fig. 8A). Figures 8B and 8C present three specific areas of a water surface denoted with the letters A, B and C. The first area represents a still water surface in which a wave train has not yet arrived. The second area shows progressive waves approaching the shore, whereas in the area denoted with the letter C, standing waves are forming as a result of superposition of the oncoming waves with the reflected ones. A noticeable disturbance of a water surface of the order of a wave height is observed at the left-hand boundary. A detailed numerical analysis, not presented here, has shown that the disturbance only appears during wave motion that is not parallel to the side boundaries. The problem can be eliminated indirectly by the proper extension of the computational domain.

The influence of a groin system on wave motion is shown in Figs. 9 and 10. The sketch of a bathymetry is given in picture 9A. A cross-section along the groin is indicated in grey. In numerical computations it has been assumed that

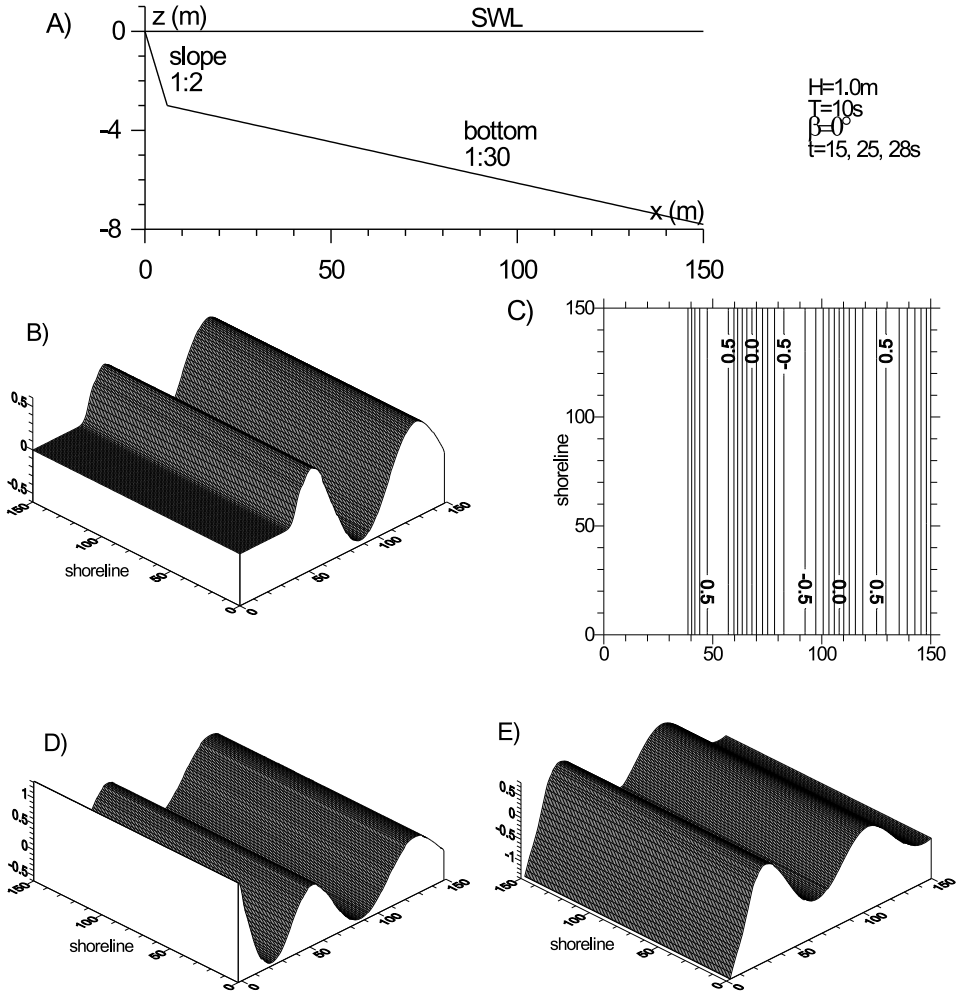

Fig. 6. Perpendicular wave approach to the shore

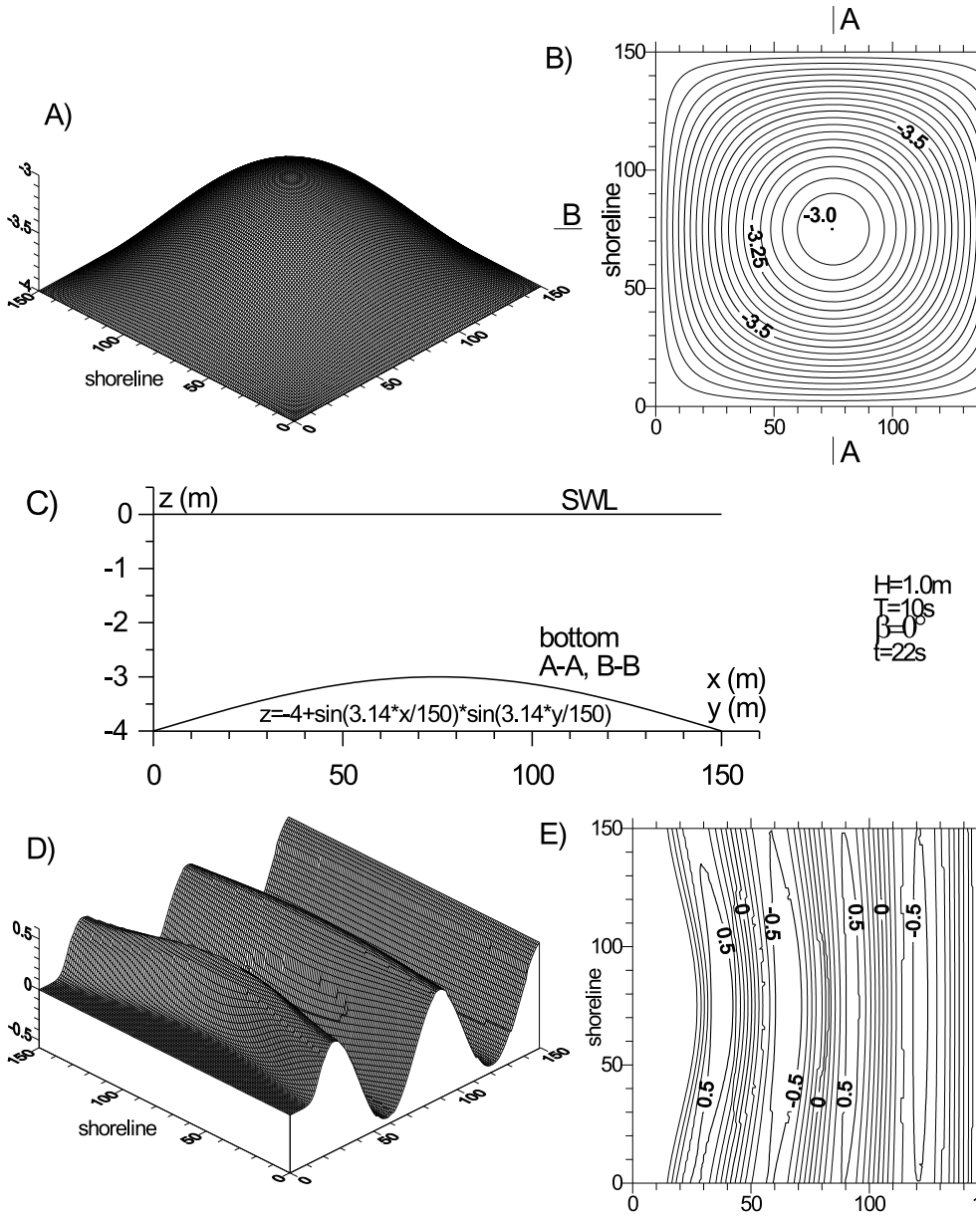

Fig. 7. Wave propagation over an underwater mound

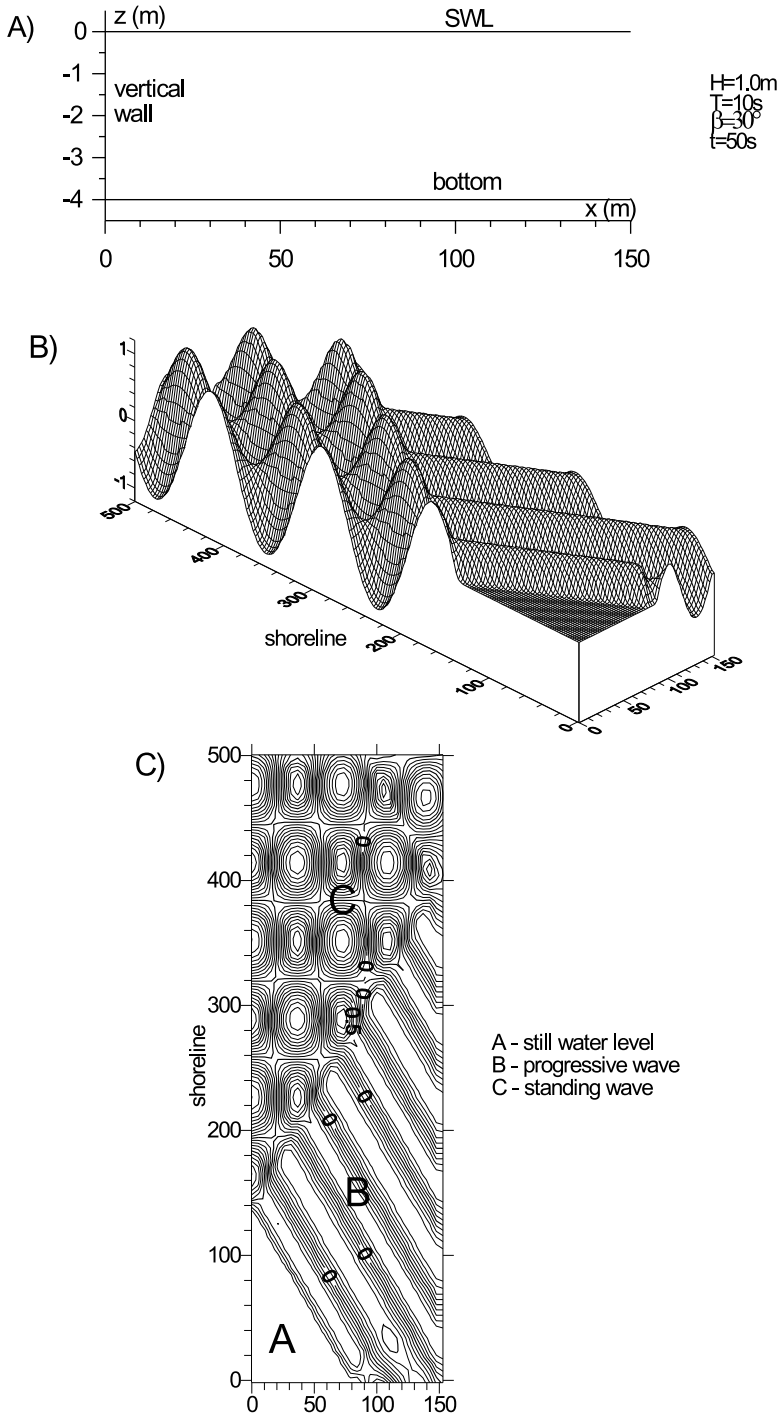

Fig. 8. Oblique wave approach to the shore

the groins are high enough to avoid wave overtopping and in addition, no wave transmission across them is possible. Figures 9B and 9C show a wave train during its propagation perpendicular to the shore. The initial phase of a standing wave formation has been caught here. In this case the groins do not influence the motion at all. Thick lines in Figs. 9B and 9C indicate locations of the groins within the computational area.

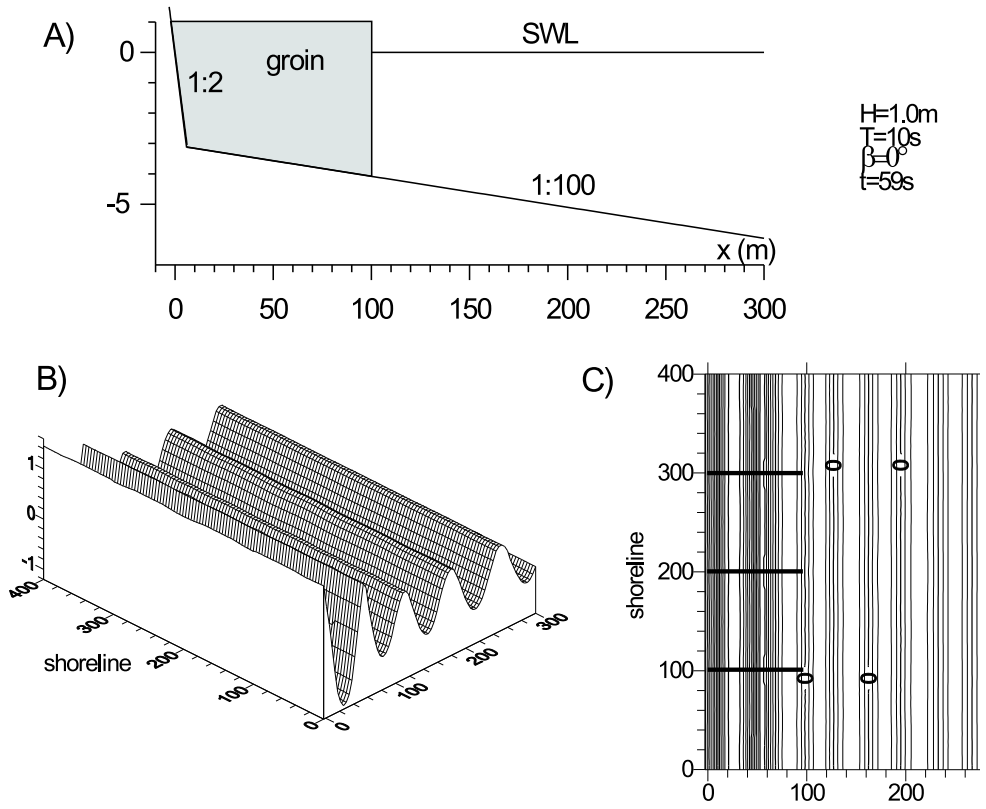

Fig. 9. Perpendicular wave run-up in the case of groins

Figures 10A through 10F show wave motion for the same conditions as in Fig. 9. The only difference is the angle of a wave approach set here at 30°. The succeeding pairs of pictures show different stages of wave motion. Propagating waves are trapped in the areas between groins and then they behave independently, compared with the neighbouring gaps. Because of a disturbance occurring on the left-hand boundary the adjacent area has to be treated with limited reliability.

The last example presents the ability of the numerical model to simulate wave diffraction caused by emerged obstacles. Figure 11 shows a wave motion in the rectangular area with a breakwater indicated with a thick line in pictures B, D and F. The 150 metre long breakwater is located 150 metres from the shoreline. In

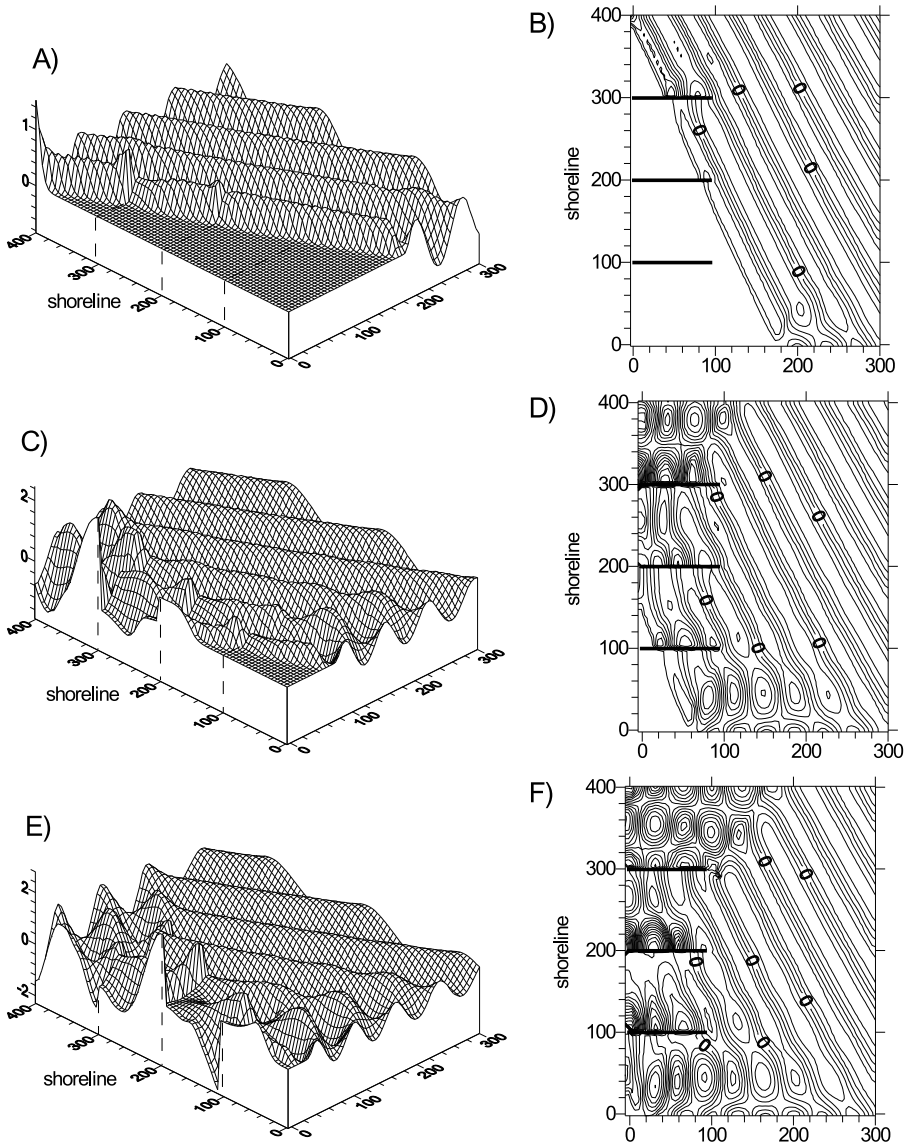

Fig. 10. Oblique wave run-up in the case of groins

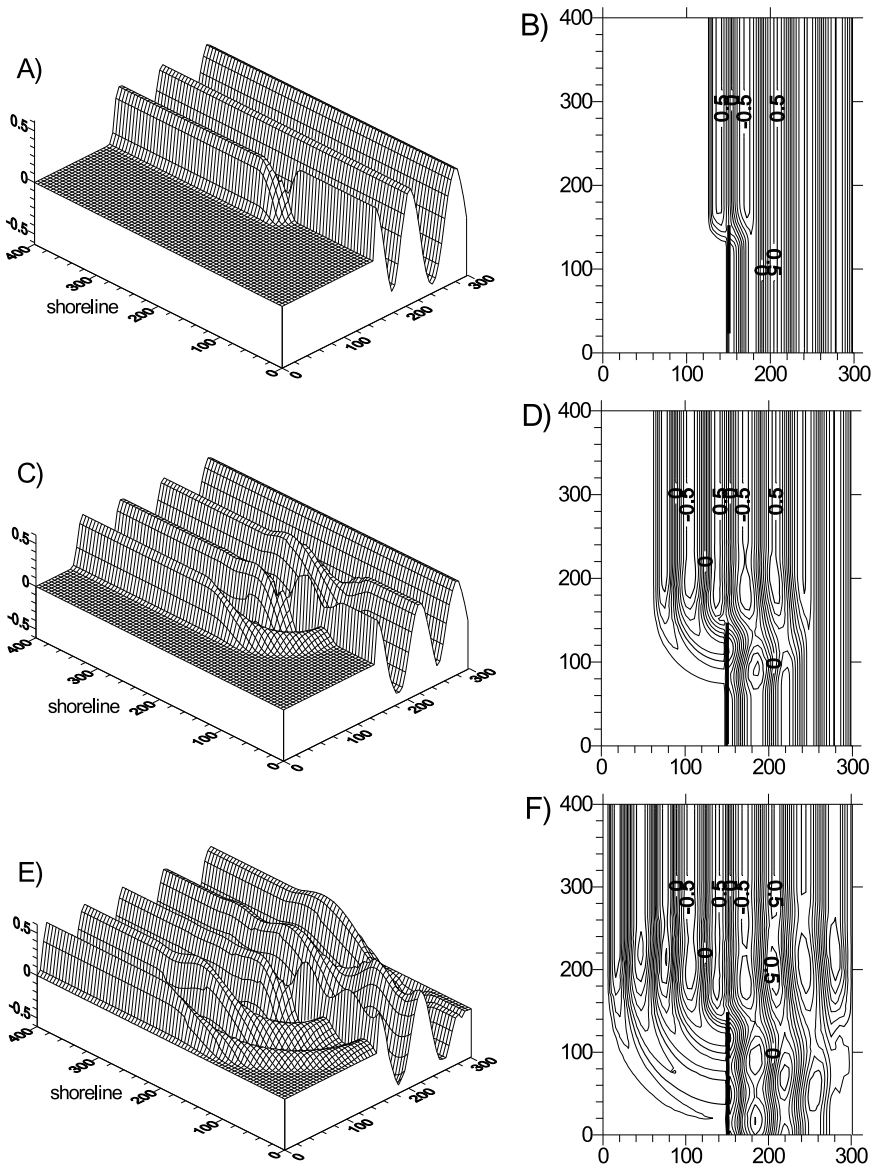

Fig. 11. Wave motion in the case of a breakwater

the model it has been assumed that landward and seaward walls are vertical and high enough to inhibit overtopping. As in the former examples, the succeeding phases of wave propagation are given in pairs. Pictures A and B show incipience of wave interruption by the breakwater, whereas in pictures E and F the waves are deep within the area sheltered by the barrier.

5. Summary

A one-dimensional model of wave motion in the hybrid Lagrangian-Eulerian description has been developed here to treat the second horizontal dimension. All properties of the preceding description have been retained. New elements in the present model are oblique propagation, diffraction and refraction of plane waves over a two-dimensional bottom. It has been proved that for the simplest case governing equations simplify the classical wave equations. For other conditions a numerical model has been elaborated. Finally, the selected results of simple numerical simulations have been presented. They show wave behaviour during propagation over both constant, and irregular bottom depths, as well as during uprush-backwash on vertical and inclined shores.

In all examples the orbital motion and mass transport were computed automatically, although they have not yet been examined. A simulation of bottom friction and wave breaking is also possible here as the analogy to the solution presented in the one-dimensional model.

References

Kapiński J. (2003), Lagrangian-Eulerian Approach to Modelling of Wave Transformation and Flow Velocity in the Swash Zone and its Seaward Vicinity, *Archives of Hydro-Engineering and Environmental Mechanics*, Vol. 50, 165–192.

Kapiński J., Kołodko J. (1996), Wave run-up on Gentle Slopes: a Hybrid Approach, *Archives of Hydro-Engineering and Environmental Mechanics*, Vol. 43, 79–89.

Potter D. (1973), *Computational Physics*, John Willey & Sons, London, New York, Sydney, Toronto.

Voltzinger N. E., Klevanny K. A., Pelinovsky E. N. (1989), *Long-Wave Dynamics of the Coastal Zone,* Gidrometeoizdat Publishers, Leningrad (in Russian).